

Effect of Seawater Chlorination on the Erosion Corrosion Behavior of Copper-Nickel Alloy CuNi90/10

W. Schleich
KME Germany AG
Klosterstr. 29, D-49023 Osnabrück, Germany
wilhelm.schleich@kme.com

R. Feser, G. Schmitt, K. Schnier, T. Gommlich, S. Günther
Laboratory for Corrosion Protection
Iserlohn University of Applied Sciences
Frauenstuhweg 31; D-58644 Iserlohn; Germany
feser.r@fh-swf.de; schmitt.g@fh-swf.de

Abstract

The influence of dissolved sodium hypochlorite on the flow resistance of UNS C70600 (CuNi90/10) in artificial ASTM D1141 seawater at room temperature was investigated gravimetrically using the rotating cage and the electrochemically controlled submerged jet impingement tests. It appeared that even under unfavorable conditions (as-delivered surface, 5 ppm hypochlorite) the critical wall shear stress for initiation of flow induced localized corrosion (FILC) reached levels of 200 Pa. Six weeks pre-exposure in hypochlorite-free artificial seawater at room temperature yields flow resistant protective scales which resist wall shear stresses up to 370 Pa (even in the presence of 5 ppm hypochlorite) without initiation of FILC. The value of 43 Pa previously reported in the literature for the critical wall shear stress of CuNi90/10 in seawater is obviously much too conservative.

Keywords: UNS C70600, CuNi90/10, seawater, chlorination, flow intensities, wall shear stress, erosion corrosion, flow induced localized corrosion, rotating cage, impinging jet, electrochemical noise

Introduction

The impact of seawater on materials performance is determined by numerous parameters such as condition of the material, system design, fabrication procedure, seawater temperature, flow intensity, biological activity, and presence of oxidizing compounds. Over several decades, many thousands of tons of copper-nickel alloys have been installed in different marine engineering structures used in the shipbuilding, offshore, power and desalination industries. CuNi90/10 is the workhorse and most widely used alloy. With its iron content of 1.5 to 2.0 wt.% (Table 1), this alloy provides optimum resistance to flowing seawater (Fig. 1).

Neither general corrosion nor pitting corrosion is a problem for CuNi90/10 in natural clean seawater or in seawater chlorinated to levels sufficient to control biological activity. However, localized corrosion may occur in polluted and stagnant seawater under conditions of deposit formation and in the presence of sulfide, which mostly originates from the activity of sulfate reducing bacteria [2-4]. Another reason for localized attack could be erosion corrosion initiated by flowing seawater. However, flow induced localized corrosion (FILC) is likely to occur only above critical local flow intensities creating local energy densities which are high enough to break down protective scales, layers or films on the metal surface [5-7]. Critical flow intensities are often given in terms of critical flow velocities. However, it has to be kept in mind that such data are not independent of geometry, e.g. the inner diameter when considering piping. Critical flow velocities in CuNi90/10 piping for seawater at 27°C were estimated to be 4.4 m/s for a tube with 0.03 m in diameter and 6.0 m/s for a tube 3 m in diameter [8]. The industrially accepted critical flow velocity in large piping for unpolluted seawater has been conservatively set in the range between 3.5 and 3.6 m·s⁻¹ [8-11].

A more general description of flow intensities is possible in terms of wall shear stresses which relate more closely to the interaction between the flowing fluid and the wall. Therefore, maximum design velocities in CuNi90/10 piping for seawater have been related to pipe diameters based on measurements of critical wall shear stresses (Fig. 2) [8]. The critical wall shear stress for the initiation of FILC on this material has been calculated to amount to 43 Pa (N/m²) [8]. Critical flow parameters for CuNi90/10 tubing are collected in Table 2. The critical flow velocities given here appear to be rather conservative. Experimental results are available which indicate that much higher flow velocities, e.g. in the range of 10 to 15 m/s, may be acceptable, specifically for emergency situations, as in fire fighting systems [12]. Even with sand loaded seawater, velocities of 7 m/s in 4" to 7" pipes yielded no appreciable corrosion attack [13].

The data given above relate to non-chlorinated seawater. It is not clear whether the presence of chlorine-containing additives will change the flow resistance of CuNi90/10 in seawater within relevant concentration ranges. Basically, it is industrially accepted that chlorine concentrations of 0.2 to 0.5 ppm exert no negative effects [4] (normally 0.25 ppm chlorine is sufficient to 100% control microbiological activity [2]). For continuous and intermittent chlorine additions, concentrations of 0.3 and 0.5 ppm, respectively, are recommended [14, 15]. All previous investigators agree on the threshold values given above and that over-chlorination should be avoided. However, they also recommend more additional research specifically on the effect of over-chlorination which presently is not sufficiently understood and experimentally backed-up.

In the first part of this project it was demonstrated [16] that the influence of chlorine on the corrosion rate under stagnant conditions is not strong and the quality of the oxide layer is not affected by the presence of chlorine. It was the aim of the present work to study the effect of chlorine-containing additive at higher concentrations on critical flow intensities to initiate FILC on CuNi90/10 in artificial seawater (ASTM D1141). The material's surface was tested both in the as-delivered and in the pre-

exposed condition. Pre-exposure for 6 weeks at room temperature in stagnant ASTM seawater produces corrosion product films known to be protective [17].

Experimental

The corrosion test system was defined to consist of standard quality CuNi90/10 soft annealed material with as-delivered and pre-exposed surfaces, artificial seawater according to ASTM D1141 with a pH of 8.2 and sodium hypochlorite as an oxidizing agent in the concentrations 0, 0.3, 0.5, 1.0, 3.0 and 5.0 ppm. The paper will concentrate on results with 0, 1 and 5 ppm hypochlorite. All experiments were performed at ambient (room) temperature with access of air to the corrosion medium.

The influence of hypochlorite additions on the critical flow intensities for initiation of FILC was evaluated both by experiments with the rotating cage and the submerged jet impingement tests. Initiation of FILC during jet impingement was indicated online via electrochemical noise diagnosis using the CoulCount software [26].

Rotating Cage Experiments

The rotating cage test (Fig. 3) is frequently used to screen the susceptibility of materials to FILC [18-20]. Due to the many experimental advantages and the successful use of rotating cage data in service, attempts have been made to quantify the flow intensities encountered at coupons rotated in the rotating cage. The Equation 1 was developed as an approximation to estimate the maximum wall shear stress at coupons in the rotating cage [19, 20]:

$$\tau_{RC} = 0.0791 \cdot Re_{RC}^{-0.3} \cdot \rho \cdot r_{RC}^2 \cdot \omega^{2.3} \quad (1)$$

where τ_{RC} is the wall shear stress in the rotating cage [Pa], Re_{RC} is the Reynolds number of the rotating cage ($Re_{RC} = \frac{\omega \cdot r_{RC}^2}{\nu}$), r_{RC} is the radius of the rotating cage [m], ρ is the solution density [$kg \cdot m^{-3}$], ω is the rotational speed [s^{-1}].

This equation is valid only for a certain geometry of the rotating cage with a certain number of coupons in a certain position without applying baffles to prevent rotation of the liquid by drag through the rotating cage.

Within a joint industry project (JIP) another set of equations has been experimentally developed to quantify local wall shear stresses at characteristic sites on coupon surfaces (Fig. 4) being rotated in the cage [21, 22]. The highest wall shear stresses were found at the inner edge in the middle of the leading edge of a rotated coupon (position 1 in Fig. 4). At this site, the mean wall shear stress can be calculated according to Equation 2, and the 95th percentile of the instantaneous wall shear stress according to Equation 3. The constants a, b and c in Equations. 3 and 4 will be reported in a future publication.

$$\tau_{mean} = a \cdot RPM^b \cdot \eta^c \quad (2)$$

$$\tau_{95} = 1.78 \cdot a \cdot RPM^b \cdot \eta^c \quad (3)$$

where RPM = revolutions per minute, η hydrodynamic viscosity [Pa s].

It appeared that critical wall shear stresses evaluated via Equation 3 match reasonably well with the critical wall shear stresses obtained via Equation 4 in jet impingement experiments. No acceptable match could be reached using Equation 1. This problem will be discussed in a future publication.

For the geometric conditions used in the rotating cage experiments during the present study, the calculated maximum wall shear stress at the inner corner in the middle of the leading edge of the rotated coupon (position 1 in Fig. 4) amounts to 200 Pa at a rotation speed of 1500 rpm.

The experimental setup in the rotating cage experiments is shown in Fig. 5. The rotating cage according to Fig. 3 was filled equidistantly with four CuNi90/10 coupons (50x10x3mm). Two of the coupons were in the as-received surface state (machined surface, finely ground, polished and degreased with acetone), while the other two coupons were in the pre-exposed surface state. Pre-exposure occurred by exposing the coupons at room temperature for 6 weeks in hypochlorite-free artificial ASTM seawater under access to air. The coupons had been weighed before mounting in the rotated cage and before pre-exposure to seawater, respectively.

The cage was positioned in a glass cylinder fitted with a thermostat and filled with 1.6 l of test liquid. The cylinder was covered with a splash lid. The duration of the test was 96 hours. At the shear stresses above the critical threshold, the mechanism of the attack is FILC and this test duration is sufficient for the detection of measurable weight losses. The cage was rotated with rotation speeds between 850 and 1500 rpm, and the test liquid was recirculated at room temperature via a recirculation pump over a chlorine/ hypochlorite electrode (model CS2.3, Sensortechnik Meinsberg GmbH, Germany), which measured the hypochlorite concentration and - via a transducer (MU2060, Sensortechnik Meinsberg GmbH) - triggered a NaOCl dosage pump which metered NaOCl solution into the test liquid to keep the hypochlorite concentration constant at 1 or 5 ppm (Fig. 6). Indicated via a digital display, the amperometric measurement yielded the concentration of "free chlorine" (including chlorine and hypochlorite) with an accuracy of 0.01 mg/. The measuring interval was 2 minutes. The electrode was calibrated with the „CHECKIT Comperator“ (Tintometer Company) using a colorimetric method. The pH of the liquid was kept constant at pH 8.2. As can be seen from the diagram in Fig. 7, the chlorine concentration at pH 8.2 is close to zero and the prevailing oxidizing compound is the hypochlorite anion and the hypochloric acid. Prior to the gravimetric measurements, the samples were cleaned in an ultrasonic bath containing 10 % aqueous citric acid solution. The microscopic examination was undertaken using a scanning electron microscope (SEM).

Electrochemical Noise Controlled Jet Impingement

Under defined flow and geometric conditions, the submerged jet develops defined wall shear stresses τ_w at impinged surfaces which can be calculated according to the empirical Equation 4 developed by Giralt and Trass [24, 25]

$$\tau_w = 0.0447 \cdot \rho \cdot u_0^2 \cdot Re^{-0.182} \left(\frac{x}{d}\right)^{-2} \quad (4)$$

where ρ is the density of the liquid [g/m^3], u_0 is the flow velocity [$\text{m}\cdot\text{s}^{-1}$], Re the Reynolds number, d the diameter of the jet nozzle [m] and x [m] the distance from the center of the jet on the impinged surface. In the jet impingement experiments with artificial seawater described in this paper the following data applied: $\rho = 1024.91 \text{ kg}/\text{m}^3$, $x = 0.003\text{m}$, $d = 0.001\text{m}$. The distance between the jet nozzle and impinged surface was 5 mm. Under these conditions, the wall shear stresses produced at different jet nozzle flow velocities on the impinged surface a distance of 3 to 5 mm from the center of the jet are exemplified in Table 3. The maximum wall shear stress achievable with the present experimental setup was 370 Pa (Table 3).

The special feature of the impinged surface applied in this investigation was that it contained two electrodes made of CuNi90/10 embedded in epoxy resin (Fig. 8 and 10). The medium-contacted surface area of each electrode was 0.725cm^2 . During jet impingement, the time-related element current flowing between the two electrodes was measured with a zero resistance ammeter (ZRA). For data evaluation,

the DC part was subtracted from the raw data and the values of the noise currents were added in short time intervals (0.05 s) yielding a total noise charge curve with a positive slope. This 'Coulombs Counting' method was developed earlier and has been reported elsewhere [26]. In the case of uniform corrosion activity on both electrodes, the time-related noise charge curve exhibits a low slope. If FILC is initiated the noise activity at the site of localized corrosion increases and, hence, the slope of the noise charge curve increases. Thus, the change of the noise charge curve indicates in real time the onset of FILC (Fig. 9).

The jet flow rig is shown schematically in Fig 11. A photo is given in Fig.12. The heart is the jet cell. A gear pump feeds test liquid from a 10 liter reservoir through a mass flow meter into the jet nozzle onto the specimen (Fig. 10). The pH, redox potential and chlorine /hypochlorite concentration are measured. The chlorine electrode triggers the feed pump for the hypochlorite addition to keep the hypochlorite concentration constant according to the same procedure as in the rotating cage experiments. A glass window allows observation of the impinged surface with a videomicroscope. The onset of localized attack can be correlated in real time with changes in the steepness of the noise charge vs. time curve.

Results and Discussion

Experiments with the Rotating Cage

Rotating cage experiments were performed to determine whether the beneficial scale effect also contributes to the level of critical wall shear stresses. Runs with rotation speeds of 850 and 1000 rpm yielded no FILC within 4 days exposure in artificial seawater regardless of the presence of hypochlorite concentrations up to 5 ppm. It needed a rotation speed of 1500 rpm to start FILC at least slightly at the leading edges of the coupons, i.e. at the sites of maximum flow intensity. This result was obtained in the absence as well as in the presence of hypochlorite up to concentrations of 5 ppm, regardless of the nature of coupon surface (as-received or pre-exposed).

As exemplified by SEM investigations shown in Fig. 13, the FLIC was only slightly visible and occurred within 30 μm of the edges. It is evident that the local flow intensities at the sharp coupon edges are higher than some 200 μm away where the microelectrodes had been implemented into the coupon surface in the previous investigations [21, 22]. Therefore, it must be assumed that the effective local wall shear stresses which finally initiated the flow induced attack directly at the edges, are considerably higher than the local wall shear stress of 200 Pa calculated for the given geometries at 1500 rpm.

Technically the equipment available was not capable of speeds which would cause shear stress to initiate FILC on a wider area of coupon surface. Therefore, jet impingement experiments were performed.

Mass loss measurements on coupons exposed at 1500 rpm clearly demonstrate that scale formation during pre-exposure to artificial seawater is beneficial for reducing the general corrosion rate at high flow intensities (Figs. 14-15). For pre-exposed surfaces, the effect of hypochlorite on the general corrosion rate is not significant up to concentrations of 5 ppm. However, for the as-received surface, the addition of small amounts of hypochlorite appears to be beneficial. Higher hypochlorite concentrations (e.g. 5 ppm), which are generally in excess of that used in practice, seem to enhance the corrosion rate again.

Experiments using the Submerged Jet Impingement Test

Electrochemical noise (ECN) control of jet impingement experiments with divided electrodes made it possible to reliably monitor in real time the onset of FILC. Figs. 16 and 17 give a typical example. When localized attack starts, on one electrode both element current and noise charge show significant

changes in the behavior of the curve with respect to noise level (Fig. 16) and steepness of the slope (Fig. 17). Videomicroscopic surface inspection proved that pit formation and change in ECN control coincided.

This method was used to evaluate critical wall shear stresses for as-delivered and pre-exposed CuNi90/10 surfaces in artificial seawater at pH 8.2 and room temperature in the absence and presence of controlled hypochlorite concentrations. Table 4 and 5 summarize the test results obtained with an as-delivered electrode surface and with a scale containing electrode surface (pre-exposure for 6 weeks in artificial seawater at room temperature).

The results show a clear dependence of the critical wall shear stress on the hypochlorite concentration (Fig. 18). An hypochlorite concentration of 5 ppm reduces the critical wall shear stress from 340 Pa (no NaOCl) to 220 Pa. However, with pre-exposed metal surfaces no localized attack could be produced at the maximum possible wall shear stress of 370 Pa, even in the presence of 5 ppm hypochlorite (Fig. 19). This indicates the high protectivity of the scale formed during pre-exposure to artificial seawater.

The general inference from these results is, that even under unfavourable conditions (as-delivered surface, 5 ppm hypochlorite) the critical wall shear stress for FILC initiation is of the order of 200 Pa, which is about five times higher than the value of 43 Pa previously reported for CuNi90/10 in artificial seawater [8]. Pre-exposure of the CuNi90/10 surface to artificial seawater at room temperature produces flow-resistant protective scales which boost the critical wall shear stress above 370 Pa, regardless of the presence of 5 ppm hypochlorite. It is documented that CuNi90/10 may suffer erosion corrosion at flow intensities below the critical threshold established in this study. It is assumed, however, that this susceptibility is attributed to the additional factors such as presence of solids in the flow. These factors play an important role for the applications of CuNi90/10 in coastal and brackish water but not offshore. However, the quantification of the synergetic effects of presence of free chlorine and solids will be a part of the future work.

Conclusions

The copper-nickel alloy UNS C70600 (CuNi90/10) exhibits excellent performance in artificial ASTM seawater at room temperature even at high flow intensities. Up to wall shear stresses of 200 Pa, only general corrosion and no flow induced localized corrosion was observed in high speed rotating cage and jet impingement experiments.

For wall shear stresses as high as 200 Pa, the flow resistance of CuNi90/10 is not impaired by hypochlorite concentrations up to 5 ppm, even on the as-delivered (not pre-exposed) metal surface. Pre-exposure for 6 weeks in artificial seawater yields protective scales which can endure wall shear stresses up to 370 Pa without initiation of FILC, regardless of hypochlorite concentrations up to 5 ppm. The results indicate that the previously reported value of 43 Pa for the critical wall shear stress of CuNi90/10 in seawater is obviously much too conservative.

The overall results of this work, including the previously reported data [16], provide no indications that the chlorination of seawater at typically applied concentrations has a negative effect on the corrosion behaviour of CuNi90/10. This is in the line with practical experience in natural seawater and can be considered as a major advantage of this material as compared with super stainless steels and some nickel-base alloys used for seawater piping systems.

Acknowledgement

The co-authors (R.F., G.S., K.S., T.G. and S.G.) thank KME Germany AG for financial support and for the permission to publish this paper.

References

1. M.S. Parvizi et al, International Materials Reviews, 33 (1988)(4) 169
2. B.C Syrett et al., Corrosion, 35 (1979)(9) 409
3. L.E. Eiselstein et al., Corros. Sci., 23 (1983) (3) 223
4. W. W. Kirk and A.H. Tuthill, Copper-Nickel Condenser and Heat Exchanger Systems, Paper from a Seminar, The Application of Copper-Nickel Alloys in Marine Systems, Presented Jointly by ICA, CDA and Nickel Development Institute in Cooperation with Japan Copper Development Association, Korean Institute of Metals, Tokyo, Osaka and Nagasaki, Japan, Pusan and Kirje Island, Republic of South Korea, November, 1991
5. G. Schmitt, C. Bosch, M. Mueller, G. Siegmund, "A Probabilistic Model for Flow Induced Localized Corrosion", CORROSION 2000, NACE International, Houston, TX, USA, 2000, Paper 049.
6. G. Schmitt, C. Werner, M. Bakalli, "Fluid Mechanical Interactions of Turbulent Flowing Liquids with the Wall - Revisited with a New Electrochemical Tool", CORROSION 005, NACE International, Houston, TX, USA, 2005, Paper 05344.
7. G. Schmitt, M. Bakalli, "Quantification of Maximum Flow Intensities in Different Flow Systems for Assessing Boundary Conditions for Flow Induced Localized Corrosion", Proc. EUROCORR'2007, 10-13 September 2007, Freiburg, Germany; DECHEMA, Frankfurt/Main, 2007.
8. K.D. Eford, Corrosion. 33 (1973) (1), 3-8.
9. J. Postlethwaite, S. Netic, "Erosion-Corrosion in Single and Multiphase Flow". In Uhlig's Corrosion Handbook, 2nd ed.; Edited by R. Winston Revie; John Wiley & Sons, Inc., 2000; Chapter 15, pp. 249-272.
10. P. Roberge, "Erosion-Corrosion". In "Corrosion Testing Made Easy", B. C. Syrett Series Editor, NACE International, Houston, TX, USA, 2004.
11. British Standard: BSMA 18, Salt Water Piping Systems in Ships, August 1973,
12. L. Knutsson et al, Brit. Corros. J., 7 (1972) 20
13. M. Jasner and K. Steinkamp, "Why Copper Nickel 90/10 is the Optimum Pipe Material for Seawater Service", Stainless Steel World 2002, Houston, USA
14. R. Francis, Materials Performance, 21 (1982)(8) 44
15. R. Francis, Corrosion, 26 (1985) (3) 205
16. W. Schleich, R. Feser, S. Siedlarek, „Electrochemical Behaviour of Copper-Nickel Alloy CuNi90/10 in Chlorinated Seawater Under Stagnating Conditions", CORROSION 2006, NACE International, Houston, TX, USA, 2006, Paper 07261
17. A Tuthill, "Guidelines for the Use of Copper Alloys in Seawater", NiDI Publication 12003. 1988
18. G. Schmitt, W. Bruckhoff, K. Faessler, G. Bluemmel, "Flow Loop versus Rotating Probes – Correlations Between Experimental Results and Service Applications", CORROSION 1990, NACE International, Houston, TX, USA, 1990, Paper 23.
19. S. Papavinasam, R.W. Revie, M. Attard, A. Demoz, H. Sun, J.C. Donini, K. Michaelian, "Inhibitor Selection for Internal Corrosion Control of Pipelines: 1. Laboratory Methodologies", CORROSION 1999, NACE International, Houston, TX, USA, Paper 1.
20. ASTM G184, "Standard Practice for Evaluating and Qualifying Oilfield and Refinery Corrosion Inhibitors using the Rotating Cage" (West Conshohocken, PA: ASTM, 2005).

21. G. Schmitt, K. Moeller, C. Werner, P. Plagemann, C. Deslouis, C. Bosch, M. J. Schöning, Y. T. Janabi, A. Belghazi, "Microturbulence Intensities in Disturbed Flow Regimes Quantified by Micro-electrochemical Measurements" Proc. 53th Ann. Meeting Intern. Soc. Electrochem. (ISE), "Electrochemistry in Molecular and Microscopic Dimensions", Düsseldorf, Germany, Sept. 15-20, 2002.
22. C. Deslouis, A. Belghazi, Y. T. Al-Janabi, P. Plagemann, G. Schmitt, "Quantifying Local Wall Shear Stresses in the Rotated Cage", CORROSION 2004, NACE International, Houston, TX, USA, 2004, Paper 727.
23. E.S.Gonçalves, L. Poulsen, P. R. Ogilby, "Polymer degradation upon exposure to chlorinated water", EUROCOR'2006, 25-28-Sept.2006, Maastricht, The Netherlands, CD-ROM European Federation of Corrosion, The Institute of Materials, London, UK.
24. F. Giralt, O. Trass, Canadian J. Chem. Eng. 53 (1975) 505-511.
25. F. Giralt, O. Trass, Canadian J. Chem. Eng. 54 (1976) 148-155.
26. G.Schmitt, R.Buschmann, K.-F. Foehn, H. Theunissen, "Bimetallic ECN Sensor for Monitoring Inhibitor Efficiency in Water-based Hydraulic Fluids", CORROSION 2005, NACE International, Houston/Texas, 2005, Paper 05-382

TABLE 1: Chemical composition (wt. %) of various specifications for cupronickel 90/10 used as piping material (single values represent the maximum content).

Standard	DIN EN 12449	ASTM B466	EEMUA 144
Designation	2.0872/CW352H	UNS C70600	UNS 7060X
Copper	Rem.	Rem.	Rem.
Nickel	9.0-11.0	9.0-11.0	10.0-11.0
Iron	1.0-2.0	1.0-1.8	1.5-2.00
Manganese	0.5-1.0	1.0	0.5-1.0
Tin	0.03	-	-
Carbon	0.05	0.05	0.05
Lead	0.02	0.02	0.01
Phosphorus	0.02	0.2	0.02
Sulfur	0.05	0.02	0.02
Zinc	0.05	0.5	0.2
Cobalt	0.1	-	-
Impurities	0.2	-	0.3

TABLE 2: Critical flow parameters for CuNi90/10 tubing in seawater [8-10].

Critical shear stress [$\text{N}\cdot\text{m}^{-2}$]	43
Critical velocity in 25 mm Tube [$\text{m}\cdot\text{s}^{-1}$]	4.3
Maximum tubular design velocity based on 50% critical shear stress [$\text{m}\cdot\text{s}^{-1}$]	2.9
Maximum tubular design velocity [$\text{m}\cdot\text{s}^{-1}$]	3.0 - 3.6

TABLE 3: Wall shear stresses at different jet nozzle flow velocities.

Flow Velocity at Jet Nozzle u_0 [m/s]	Mass Flow [g/s]	Wall Shear Stress τ_w [Pa]
9	7.2	80
12	9.7	135
15	12.1	200
18	14.5	280
21	16.9	370

TABLE 4: Jet impingement experiments with CuNi90/10 surfaces in as-delivered condition in artificial seawater at room temperature - effect of hypochlorite concentration.

Hypochlorite Concentration [ppm]	Wall Shear Stress [Pa]	Exposure Time [h]	FILC	Remarks
0,0	300	52	Yes	Start of FILC after 500 min
	280	168	No	-
	220	504	No	-
	200	96	No	-
1,0	300	10	Yes	Start of FILC after 5 min
	280	10	Yes	Start of FILC after 80 min
	260	168	No	-
5,0	300	10	Yes	Start of FILC after 10 min
	280	10	Yes	Start of FILC after 40 min
	220	10	Yes	Start of FILC after 15 min
	200	504	No	-

TABLE 5: Jet impingement experiments with CuNi90/10 surfaces in pre-exposed condition in artificial seawater at room temperature - effect of hypochlorite concentration.

Hypochlorite Concentration [ppm]	Wall Shear Stress [Pa]	Exposure Time [h]	FILC	Remarks
0,0	340	120	No	-
1,0	340	120	No	-
	300	120	No	-
	220	336	No	3 weeks exposure under 220 Pa wall shear stress
5,0	340	96	No	-
	300	120	No	-
	240	120	No	-
	220	336	No	5 weeks exposure under 220 Pa wall shear stress

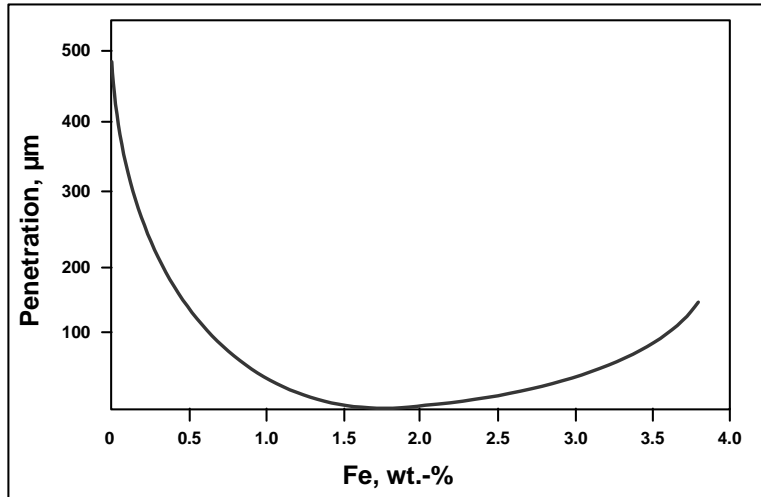


FIGURE 1: Influence of iron content on depth of impingement attack on CUNI90/10 in seawater after 30 days exposure at 3 m/s [1].

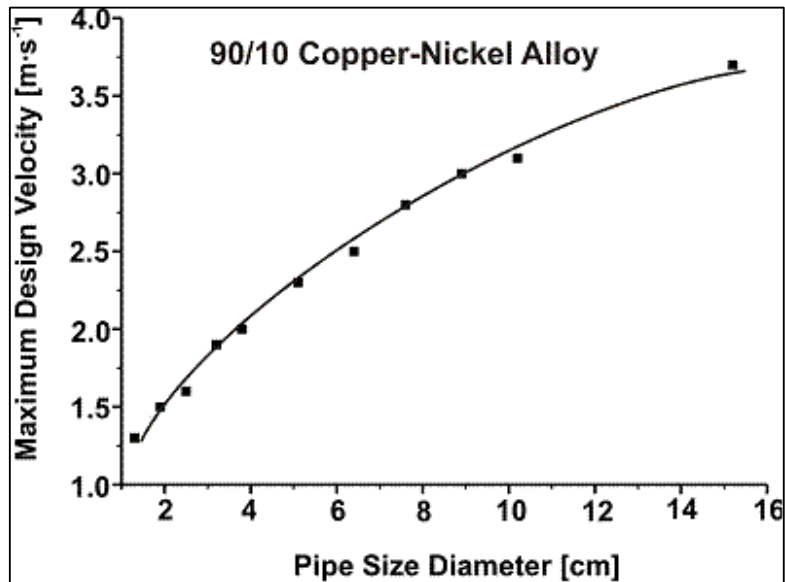


FIGURE 2: Maximum design velocities of CuNi90/10 piping for seawater [8].

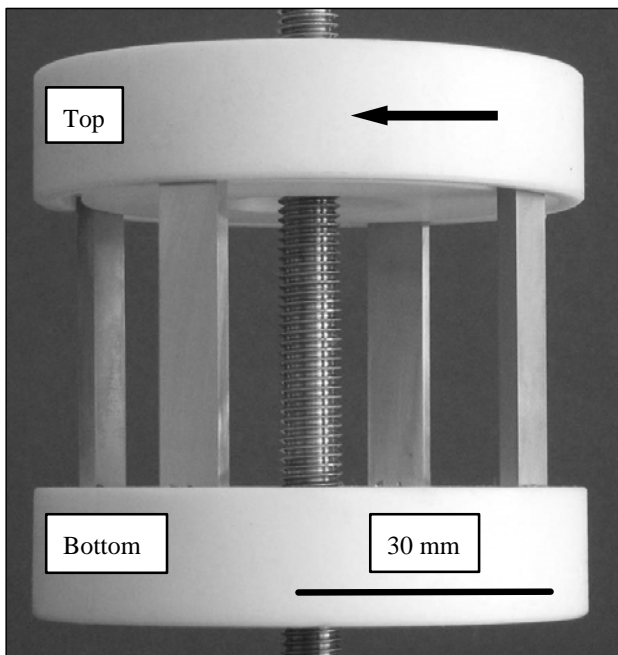


FIGURE 3: Rotating cage.

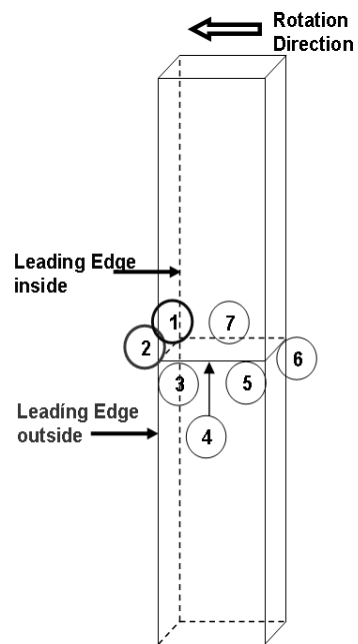


FIGURE 4: Characteristic surface sites on coupons being rotated in the cage [23, 24].

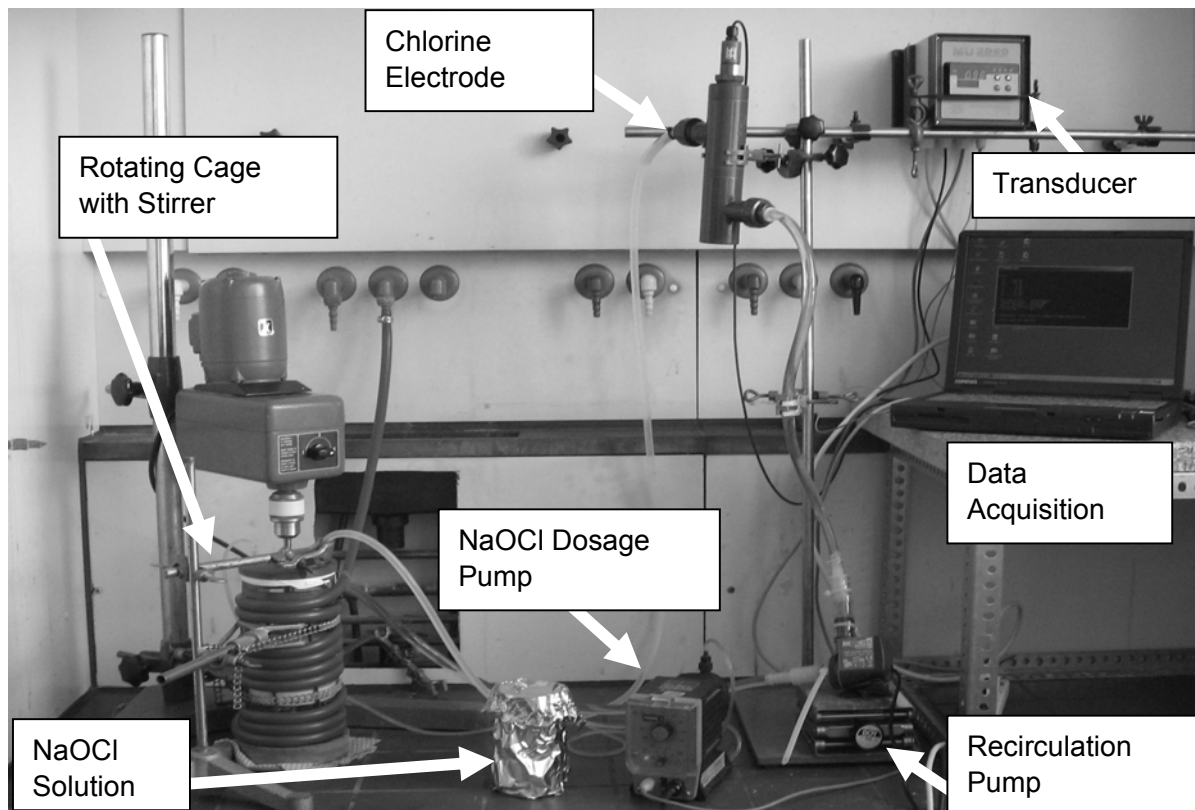


FIGURE 5: Experimental setup for rotating cage experiments in NaOCl-containing artificial seawater.

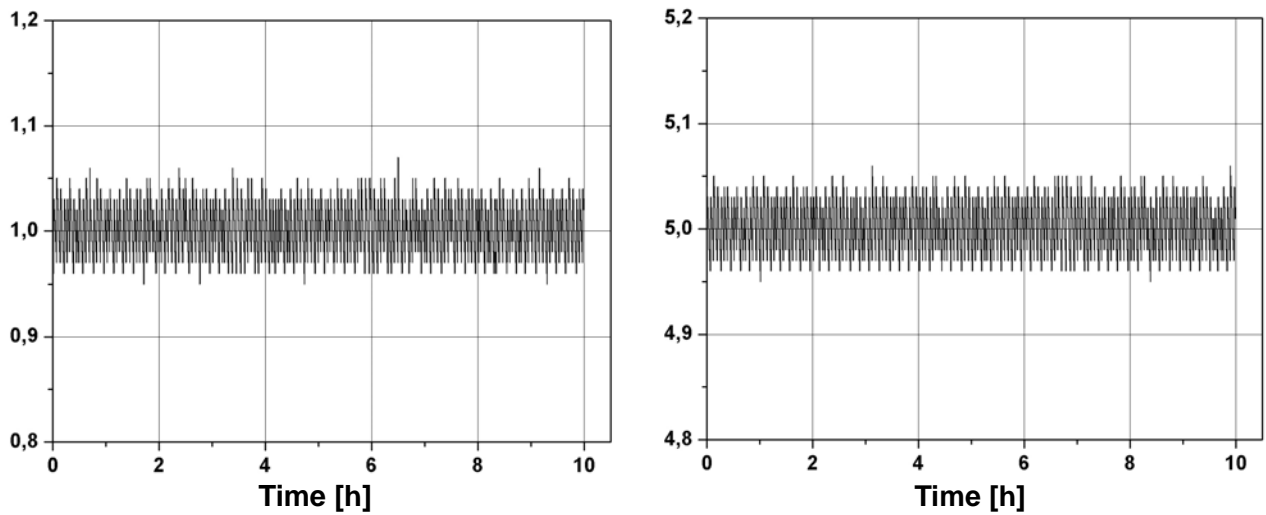


FIGURE 6: Recordings of hypochlorite concentration in the test liquid (examples for runs with 1 ppm and 5 ppm hypochlorite).

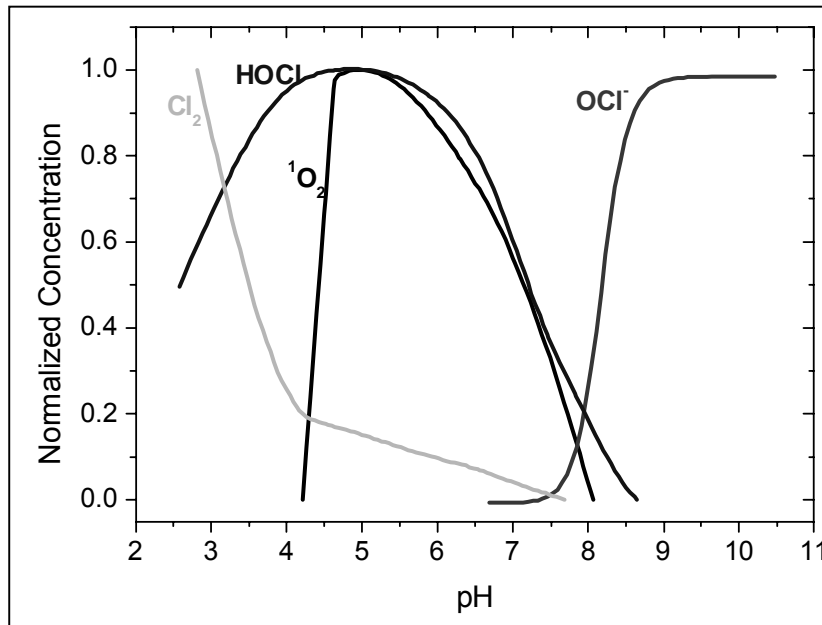


FIGURE 7: Effect of pH on chlorine concentration in hypochlorite-containing waters [23].

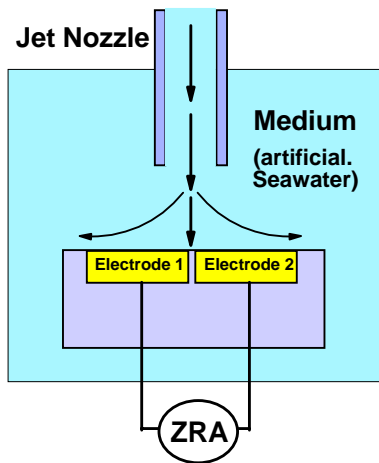


FIGURE 8: Sketch of the experimental setup in jet impingement experiments.

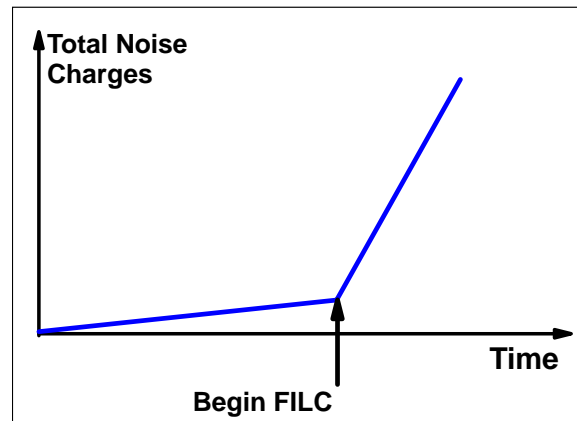


FIGURE 9: Increase in total noise charges vs. time curve indicates onset of SILC.

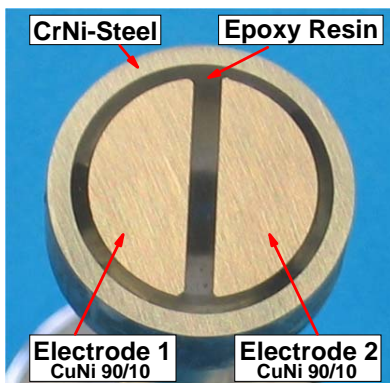


FIGURE 10: Jet impinged surface with two CuNi90/10 electrodes embedded in epoxy resin.

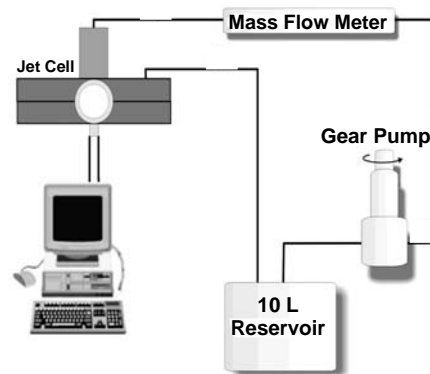


FIGURE 11: Sketch of the jet impingement flow rig.

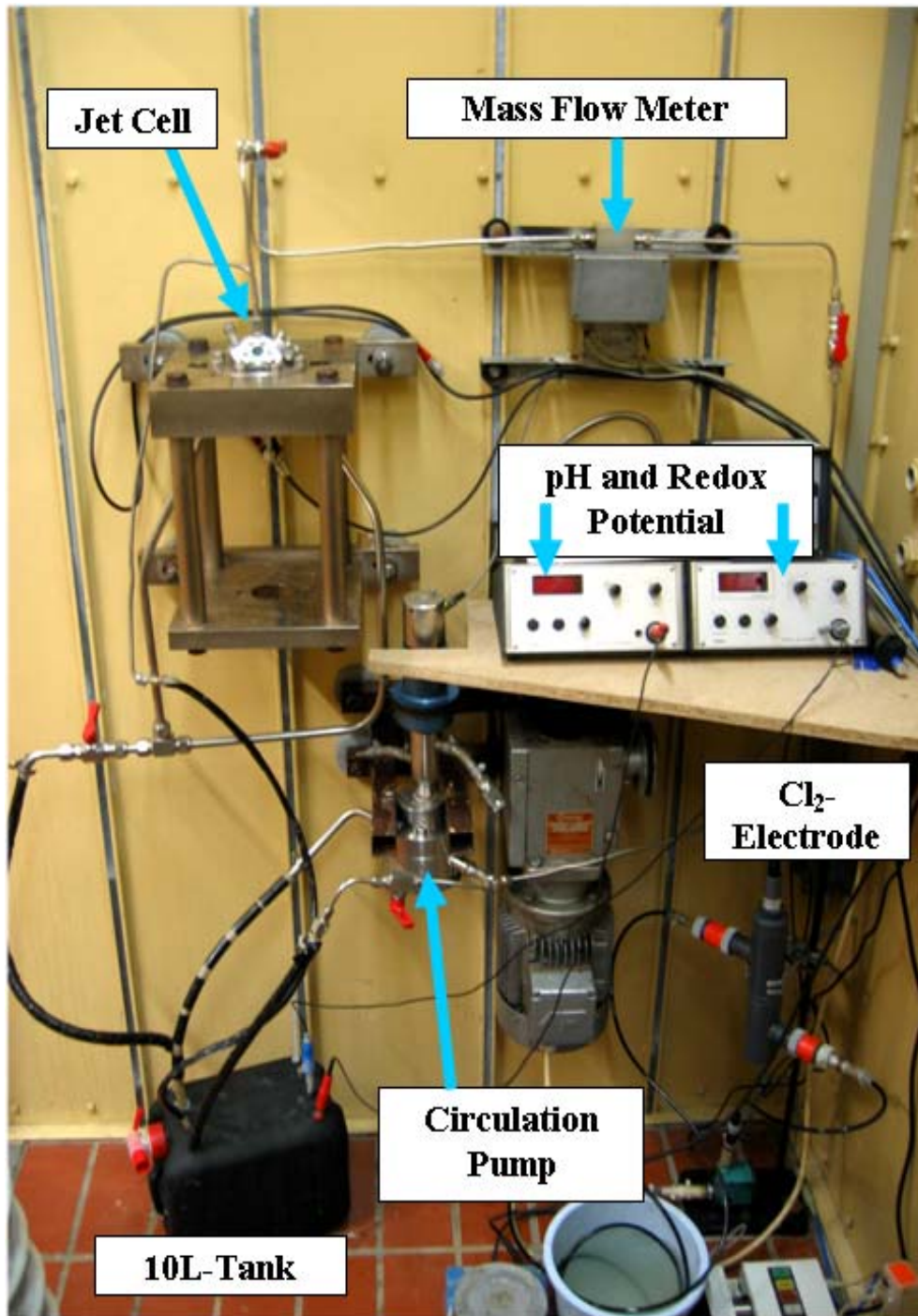


FIGURE 12: Jet flow rig including sodium hypochlorite pump triggered by Cl₂-electrode.

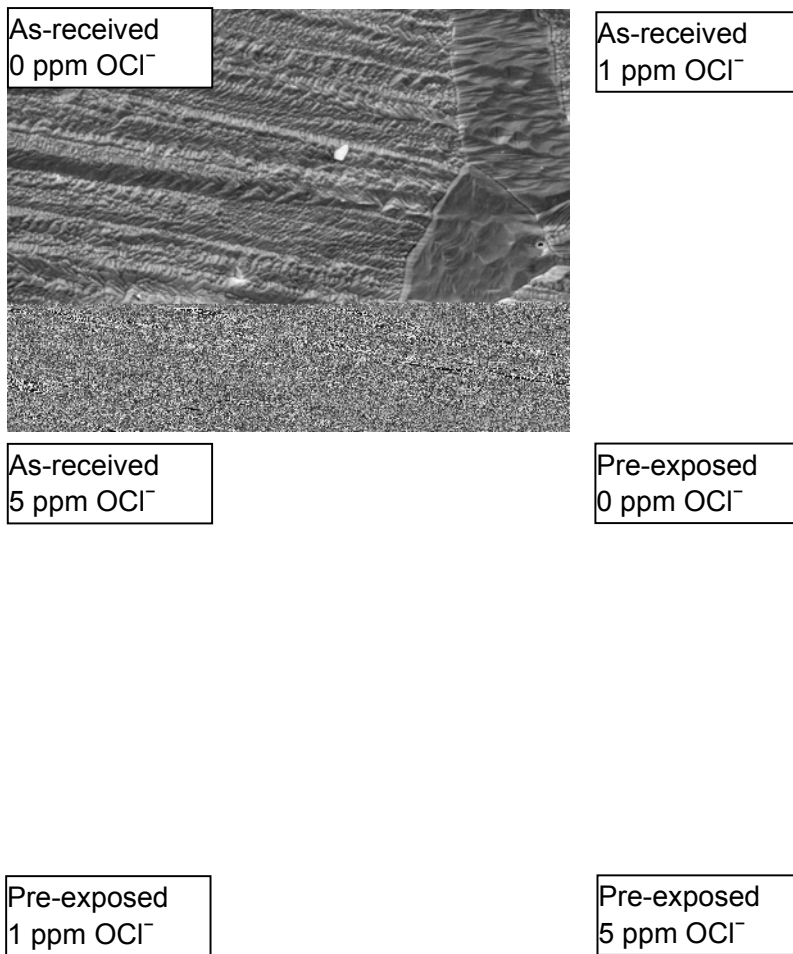


FIGURE 13: Effect of pre-exposure and presence of hypochlorite on the onset of flow induced localized corrosion of CuNi90/10 coupons rotated in at 1500 rpm for 4 days in artificial seawater at room temperature and the etching of the sample surface.

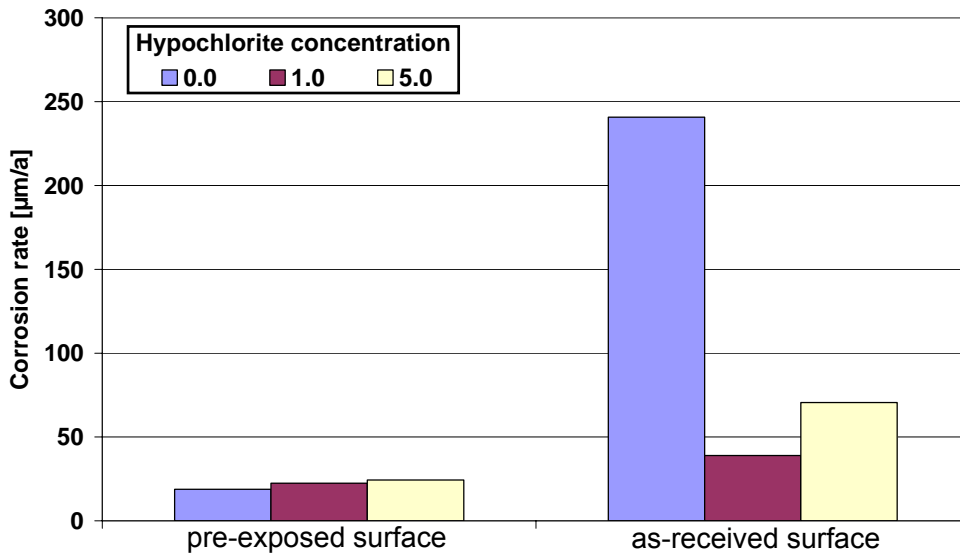


FIGURE 14: Effect of pre-exposure and presence of hypochlorite on corrosion rate of CuNi90/10 coupons after 4 days rotation at 1500 rpm in artificial ASTM seawater at room temperature.

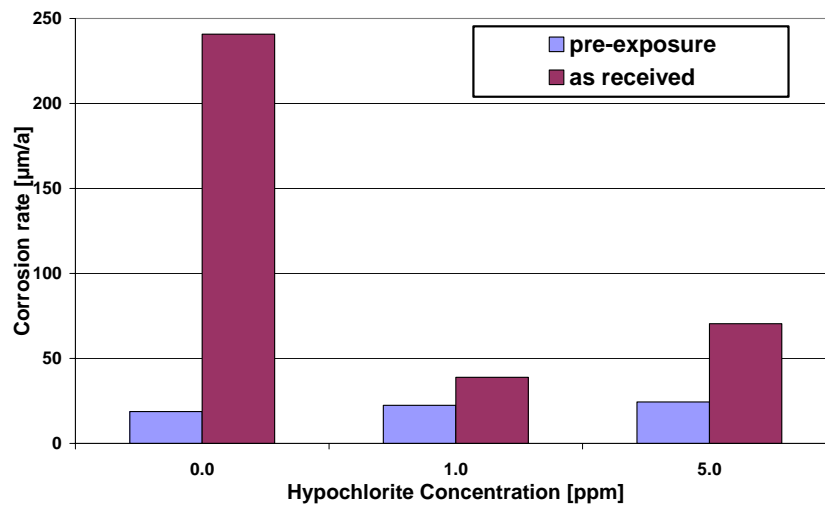


FIGURE 15: Effect of pre-exposure and presence of hypochlorite on corrosion rate of CuNi90/10 coupons after 4 days rotation at 1500 rpm in artificial ASTM seawater at room temperature.

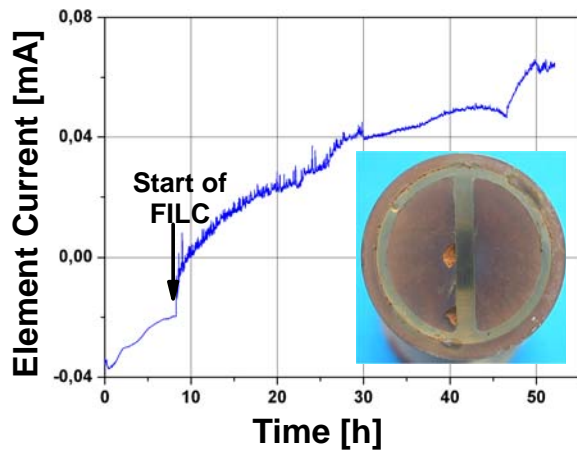


FIGURE 16: ECN controlled jet impingement test - Response of element current.

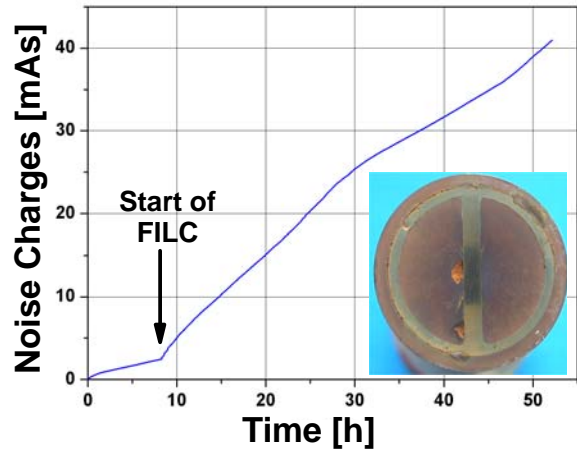


FIGURE 17: ECN controlled jet impingement test - Response of noise charges.

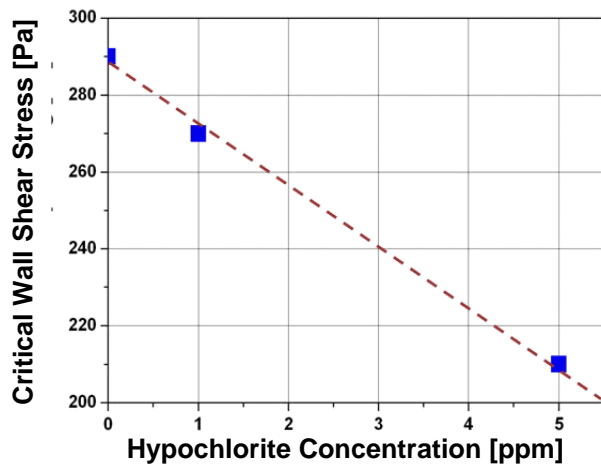


FIGURE 18: Effect of hypochlorite concentration on critical wall shear stresses at CuNi90/10 (as-delivered surface) in artificial seawater at room temperature.



FIGURE 19: Electrode surfaces after 5 weeks under 370 Pa jet impingement at room temperature with artificial seawater containing 5 ppm hypochlorite.